Molecular Therapy
Original Article

Targeting choroidal vascular dysfunction via inhibition of circRNA-FoxO1 for prevention and management of myopic pathology

Dan Li,[1,2,5] Chang Liu,[3,4,5] Ya-Nan Sun,[1,2,5] Chuan-Yan Zhu,[3,4,5] Shan-Shan Xu,[3,4] Kun Shan,[1,2] Shu-Jie Zhang,[1,2] Biao Yan,[1,2] and Yi Lu[1,2]

[1]Eye Institute, Eye & ENT Hospital, Shanghai Medical College, Fudan University, Shanghai, China; [2]NHC Key Laboratory of Myopia (Fudan University), Key Laboratory of Myopia, Chinese Academy of Medical Sciences, and Shanghai Key Laboratory of Visual Impairment and Restoration (Fudan University), Shanghai, China; [3]The Affiliated Eye Hospital, Nanjing Medical University, Nanjing, China; [4]The Fourth School of Clinical Medicine, Nanjing Medical University, Nanjing, China

Myopia has become a global public health problem due to high prevalence. Although the etiological factors of myopia have been gradually recognized, the underlying mechanism remains largely elusive. Choroidal vascular dysfunction is recognized as a critical vision-threatening complication in myopia. Circular RNAs (circRNAs) are shown as the critical regulators in many biological processes and human diseases. In this study, we investigated the role of circRNAs in choroidal vascular dysfunction in myopia. The level of circFoxO1 was significantly upregulated in myopic choroid. circFoxO1 silencing suppressed choroidal endothelial cell viability, proliferation, migration, and tube formation *in vitro* and alleviated choroidal vascular dysfunction *in vivo* and *ex vivo*. circFoxO1 silencing retarded the progression of myopia as shown by reduced extracellular matrix remodeling and improved refractive error and axial elongation. Mechanistically, circFoxO1 acted as the sponge of miR-145 to sequester and inhibit miR-145 activity, thereby inducing VEGFA or ANGPT2 expression. miR-145 could mimic the effects of circFoxO1 silencing on choroidal endothelial phenotypes. Collectively, intervention of choroidal vascular dysfunction via regulating circFoxO1 level is a potential strategy for the prevention and management of myopia.

INTRODUCTION

Myopia has gradually become a global public health problem due to its high prevalence.[1,2] The rising prevalence of myopia, especially high myopia, can increase the risk of vision impairment and induce irreversible ocular complications.[3] Many strategies have been proposed for the treatment of myopia, such as spectacle lenses, refractive surgery, orthokeratology, and pharmacological treatment (i.e., atropine eye drops).[4,5] However, these strategies were only designed for the correction of optical consequences of myopia rather than targeting the molecular pathogenesis of myopia. Moreover, the cost of myopia treatment is increasing constantly, which has become a considerable economic burden in developing countries.[6] Hence, it is urgent to clarify the molecular mechanism of myopia and search for novel treatment alternatives.

The pathogenesis of myopia is tightly associated with ocular axial elongation and scleral extracellular matrix (ECM) remodeling.[7,8] The sclera is a dense and fibrous connective tissue, which can support the retina and protect ocular content against external trauma.[9] Choroid vessels supply oxygen and nutrients to the outer retina and the overlying sclera.[10] Clinical evidence has shown that reduction of choroidal vascular component is closely correlated with the severity of myopia.[11] Decreased perfusion or vascular dysfunction leads to inadequate oxygen supply and tissue hypoxia. Hypoxia is identified as the critical inducer of ECM remodeling.[12] Hypoxia contributed to the transdifferentiation of fibroblasts into myofibroblasts, resulting in decreased collagen production and ocular axial elongation.[9] Based on the above-mentioned evidence, we speculate that choroidal vascular dysfunction may occur before scleral ECM remodeling. Targeting choroidal vascular dysfunction may provide a novel therapeutic strategy for myopia.

Circular RNAs (circRNAs) have emerged as a class of non-coding RNAs that are generated via the back-splicing mechanism. They are resistant to ribonucleases and more stable than linear transcripts due to the closed-loop structures.[13] They are usually conserved across different species and stably expressed in tissue/developmental stage-specific manners.[14] They can regulate gene expression by acting as microRNA (miRNA) sponges, transcriptional regulators, and protein-like regulators.[13,15] Aberrant circRNA expression has been implicated in many human disorders, such as neurological diseases,[16] cardiovascular diseases,[17] and cancers.[18] Collectively, circRNAs are shown as the promising targets for therapeutic intervention and

Received 23 September 2020; accepted 24 February 2021;
https://doi.org/10.1016/j.ymthe.2021.02.025.

[5]These authors contributed equally

Correspondence: Biao Yan, Eye Institute, Eye & ENT Hospital, Shanghai Medical College, Fudan University, #83 Fen Yang Road, Shanghai 200030, China.
E-mail: biao.yan@fdeent.org
Correspondence: Yi Lu, Eye Institute, Eye & ENT Hospital, Shanghai Medical College, Fudan University, #83 Fen Yang Road, Shanghai 200030, China.
E-mail: luyieent@126.com

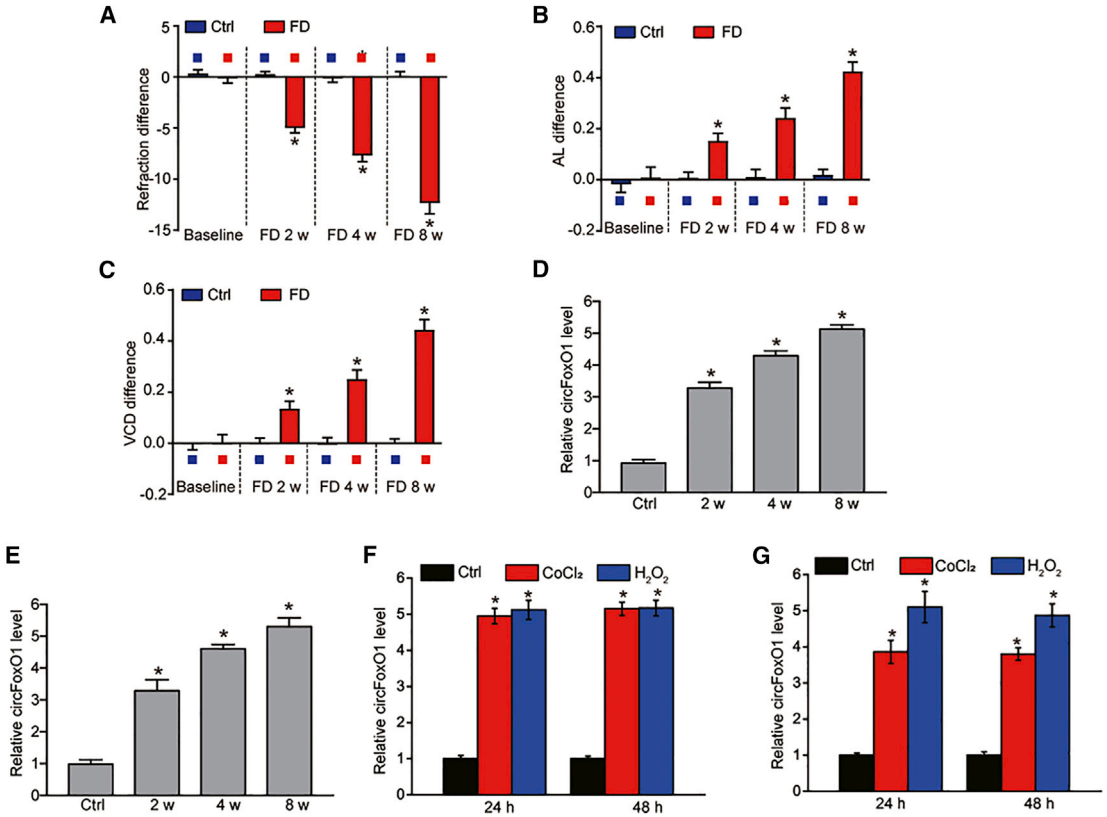

Figure 1. Myopia leads to an increased level of circFoxO1 during choroidal vascular dysfunction

(A–C) The guinea pigs underwent monocular form deprivation (FD) using the translucent eye shield. Three ocular biometric parameters, including refractive state (A), axial length (AL; B), and vitreous chamber depth (VCD; C), were measured to verify the successful establishment of a myopia model (n = 6 retinas per group; Mann-Whitney U, Bonferroni test). (D) qRT-PCR assays were conducted to detect the expression of circFoxO1 in the choroidal samples of guinea pigs after 0 (control [Ctrl]), 2, 4, or 8 weeks of FD treatment (n = 6 retinas per group; Kruskal-Wallis test, Bonferroni test). (E) qRT-PCR assays were conducted to detect the expression of circFoxO1 in the choroid of C57BL/6 mice after 0 (Ctrl), 2, 4, or 8 weeks of FD treatment (n = 6 retinas per group; Kruskal-Wallis test, Bonferroni test). (F and G) circFoxO1 expression was detected by qRT-PCRs in RF/6A cells or primarily isolated choroidal endothelial cells (ECs) cultured in the medium containing normal medium (Ctrl), $CoCl_2$ (200 μM), or H_2O_2 (100 μM) for 24 and 48 h (n = 4; *p < 0.05 versus Ctrl group, one-way ANOVA, Bonferroni test).

disease diagnosis. However, the functional significance of circRNA in choroidal vascular dysfunction in myopia is still unclear.

In this study, we investigated the role of circRNA in choroidal vascular dysfunction in myopia. The level of circFoxO1 was found to be significantly increased in myopic choroid. circFoxO1 silencing suppressed choroidal vascular dysfunction and retarded the progression of myopia. Intervention of choroidal vascular dysfunction via regulating the circFoxO1 level may be a promising strategy for the prevention and management of myopic pathology.

RESULTS

Myopia leads to an increased level of circFoxO1 during choroidal vascular dysfunction

Guinea pigs underwent form deprivation (FD) in one eye for 2, 4, and 8 weeks to induce experimental myopia. The fellow eye was taken as the control (Ctrl). Ocular biometric parameters, including eye refraction, axial length (AL), and vitreous chamber depth (VCD) of guinea pigs were detected. We did not observe the significant differences of ocular biometric parameters between FD eyes and the control eyes at the beginning of FD. The FD eyes developed experimental myopia after the treatment of FD for 2, 4, and 8 weeks as shown by increased refraction error, axial prolongation, and VCD compared with the control eyes (Figures 1A–1C).

Cellular and functional changes that occur in the choriocapillaris play a critical role in the pathogenesis of myopia,[19] We thus determined whether the level of circFoxO1 was significantly altered in the choroid of myopic guinea pigs. qRT-PCR assays showed that the level of circFoxO1 was significantly upregulated in myopic choroid compared with normal choroid in guinea pigs (Figure 1D). Although it was difficult to measure the ocular biometrics of C57BL/6 mice, we also conducted FD treatment to induce myopic shift in C57BL/6 mice. qRT-PCR assays revealed that the level of circFoxO1 was also upregulated in myopic choroid compared with normal choroid in C57BL/6 mice (Figure 1E).

Endothelial cells (ECs) are the major cell types of choriocapillaris. Rhesus choroid-retinal endothelial (RF/6A) cells or mouse choroidal ECs (CECs) were exposed to hypoxic stress or oxidative stress to mimic myopia-related pathological stresses.qRT-PCR assays showed that the level of circFoxO1 was significantly upregulated in RF/6A cells or choroidal ECs upon hypoxic stress or oxidative stress (Figures 1F and 1G). Given the induction of circFoxO1 in myopia, we examined the role of circFoxO1 in the progression of myopia in the following study.

circFoxO1 regulates choroidal EC function *in vitro*

To determine the role of circFoxO1 in choroidal ECs *in vitro*, RF/6A cells were transfected with circFoxO1 small interfering RNA (siRNA) or circFoxO1 vector to regulate circFoxO1 levels. Compared with the control group, circFoxO1 silencing by circFoxO1 siRNA led to a reduced level of circFoxO1. circFoxO1 overexpression led to an increased level of circFoxO1 in RF/6A cells (Figure 2A). We then investigated the role of circFoxO1 in RF/6A cells *in vitro*. MTT (3-(4,5-dimethylthiazol-2-yl)-2,5-diphenyltetrazolium bromide) assays showed that circFoxO1 silencing led to reduced cell viability (Figure 2B). EdU (5-ethynyl-2′-deoxyuridine) assays showed that circFoxO1 silencing significantly decreased the proliferation ability of RF/6A cells (Figure 2C). Transwell and Matrigel tube formation assays showed that circFoxO1 silencing significantly reduced the migration ability and tube formation ability of RF/6A cells (Figures 2D and 2E). We also determined whether circFoxO1 overexpression was capable of driving endothelial angiogenic phenotypes. The results showed that circFoxO1 overexpression led to increased viability, proliferation, migration ability, and tube formation ability of RF/6A cells (Figure S1).

Moreover, we also determined the role of circFoxO1 in primarily isolated choroidal ECs. MTT assays showed that circFoxO1 silencing led to reduced viability of choroidal ECs. EdU assays showed that circFoxO1 silencing decreased the proliferation ability of choroidal ECs. Transwell and Matrigel tube formation assays showed that circFoxO1 silencing reduced the ability of migration and tube formation of choroidal ECs (Figure S2). We also found that circFoxO1 overexpression was capable of driving endothelial angiogenic phenotypes of choroidal ECs. circFoxO1 overexpression led to increased viability, proliferation, migration, and tube formation (Figure S3).

circFoxO1 silencing inhibits choroidal vascular dysfunction *in vivo* and *ex vivo*

Based on the above-mentioned evidence, we knew the critical role of circFoxO1 in choroidal ECs. We then determined whether circFoxO1 played an important role in choroidal vascular dysfunction. We first used laser-induced choroidal neovascularization (CNV) model to examine the role of circFoxO1. C57BL/6J mice received an intravitreal injection of circFoxO1 short hairpin RNA (shRNA) or scrambled (Scr) shRNA for 2 weeks. We designed three different shRNAs to reduce circFoxO1 level. qRT-PCR assays showed that the levels of circFoxO1 in the choroid were significantly reduced after circFoxO1 shRNA injection. However, the levels of FoxO1 mRNA were not altered in the choroid after circFoxO1 shRNA injection (Figure 3A). circFoxO1 shRNA1 was chosen for the subsequent experiment due to its highest silencing efficiency. Isolectin B4 (IB4) immunofluorescence staining revealed that circFoxO1 silencing led to decreased neovascular area in the choroidal flat mounts compared with Scr shRNA-injected group (Figure 3B). We then used the choroidal sprouting model to determine the role of circFoxO1 *ex vivo*. The choroid explants were embedded in Matrigel and stained by CD31 at days 4, 5, and day 6 after *ex vivo* incubation. The results showed that circFoxO1 silencing led to decreased sprouting ability of choroidal ECs (Figure 3C). Collectively, these results suggests that circFoxO1 plays an important role in the development of CNV.

circFoxO1 silencing retards the progression of myopia *in vivo*

Choroidal vascular dysfunction can affect the progression of myopia.[20] We then investigated whether circFoxO1 was involved in the pathogenesis of myopia. We designed three different shRNAs to reduce circFoxO1 levels in the choroid of guinea pigs. Two shRNAs could reduce the level of circFoxO1 in the choroid. Of them, shRNA1 had a greater silencing efficiency. In contrast, the injection of circFoxO1 shRNA3 had no effect on the expression levels of FoxO1 mRNA (Figure 4A). circFoxO1 silencing led to improved refractive errors compared with Scr shRNA-injected eyes at 2, 4, and 8 weeks after FD treatment (Figure 4B). circFoxO1 silencing also retarded the elongation of AL (Figure 4C) and VCD (Figure 4D). Altered refraction error and elongation of VCD and AL are tightly associated with reduced collagen synthesis and myofibroblast transdifferentiation in sclera.[21,22] Western blots showed that myopia led to reduced expression of a fibroblast marker (COL1α1) and increased expression of myofibroblast markers (α-SMA and vinculin) in the sclera at 8 weeks after FD treatment. circFoxO1 silencing could also reverse the downregulation of a fibroblast marker (COL1α1) and the upregulation of myofibroblast markers (α-SMA and vinculin) in the sclera (Figure 4E). Immunofluorescence staining further verified that circFoxO1 silencing restored scleral collagen production and inhibited myofibroblast transdifferentiation in myopic eyes (Figure 4F). Taken together, these results suggest that circFoxO1 silencing retards the progression of myopia *in vivo*.

circFoxO1 acts as a miRNA sponge in choroidal ECs

Accumulating evidence has shown that circRNAs usually play their roles by acting as the miRNA sponges.[23] qRT-PCR revealed that circFoxO1 was mainly in cytoplasm but not in nucleus (Figure 5A). We then used the circRNA database to predict the potential miRNAs that could bind to circFoxO1. To validate the binding capability of miRNAs to circFoxO1, we constructed a circFoxO1 luciferase reporter system. Each predicted miRNA mimic was co-transfected with circFoxO1 luciferase reporter into HEK293T cells. The results showed that miR-145 mimic and miR-486-3p mimic were capable of reducing the luciferase activity of circFoxO1-Luc. Notably, miR-145 could reduce by about 80% luciferase activity of circFoxO1-Luc (Figure 5B). In contrast, miR-145 mimic transfection did not affect the luciferase activity of circFoxO1-Luc mutant without miR-145 binding sites (Figure 5C). The potential binding sites between miR-145 and circFoxO1 are shown in Figure 5D.

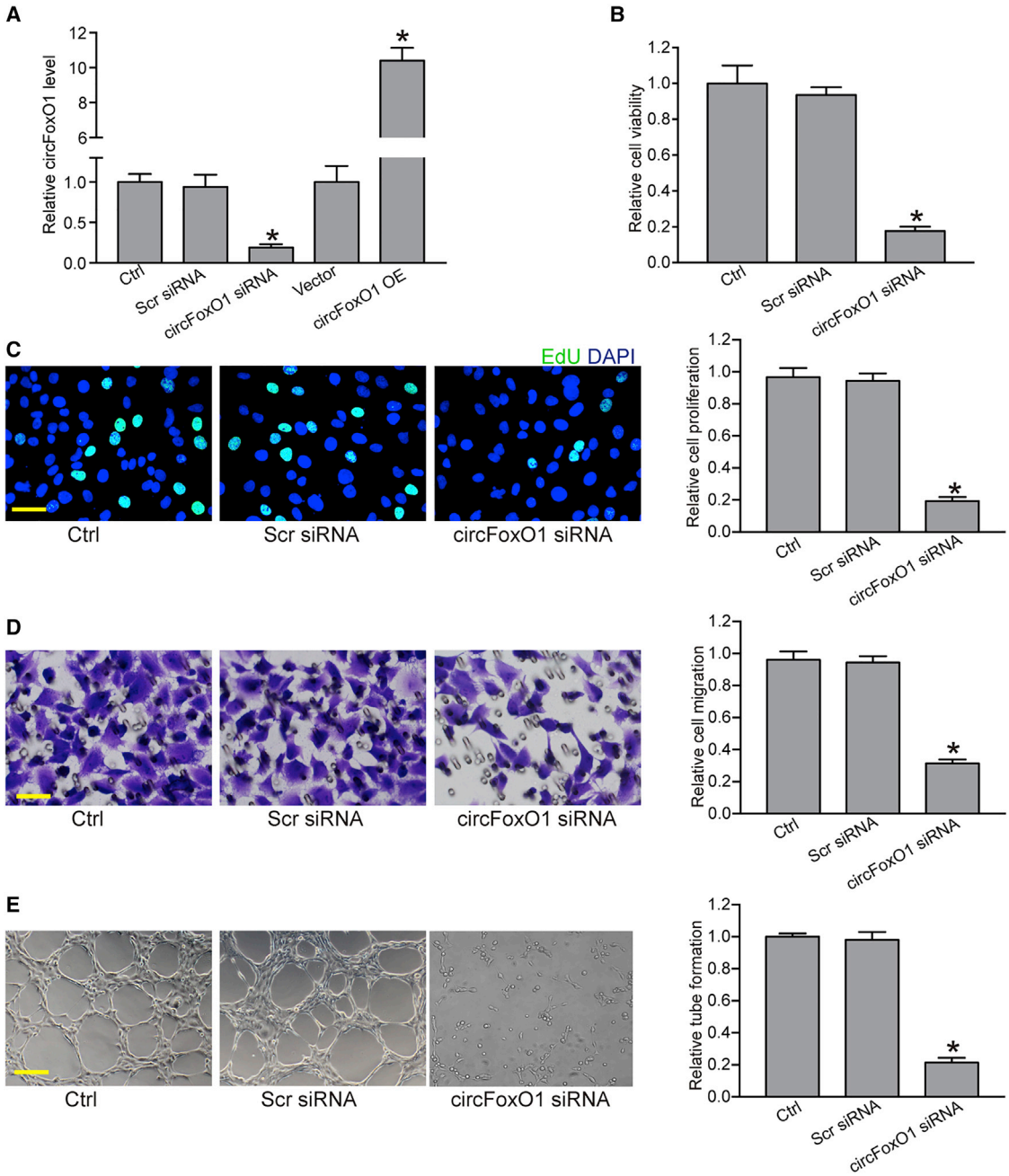

Figure 2. circFoxO1 regulates choroidal EC function *in vitro*

(A) RF/6A cells were transfected with scrambled (Scr) siRNA, circFoxO1 siRNA, pcDNA 3.1 vector, pcDNA 3.1-circFoxO1 (circFoxO1 OE), or were left untreated (Ctrl) for 48 h. qRT-PCR assays were conducted to detect the levels of circFoxO1 ($n = 4$; $^*p < 0.05$ versus Ctrl group, one-way ANOVA, Bonferroni test). (B–E) RF/6A cells were transfected with Scr siRNA, circFoxO1 siRNA, or were left untreated (Ctrl) for 48 h. Cell viability was detected using an MTT assay (B, $n = 4$; $^*p < 0.05$ versus Ctrl group, one-way ANOVA, Bonferroni test). Cell proliferation was detected using an EdU detection kit to analyze the incorporation of EdU during DNA synthesis (C, $n = 4$; $^*p < 0.05$ versus Ctrl group, one-way ANOVA, Bonferroni test). Scale bar, 20 μm. Cell migration was determined using the transwell assay, and the cells that migrated through the transwell were quantified (D, $n = 4$; $^*p < 0.05$ versus Ctrl group, one-way ANOVA, Bonferroni test). Scale bar, 20 μm. RF/6A cells were seeded on the Matrigel matrix. The tube-like structures were observed 6 h after cell seeding. The average length of tube formation for each field was statistically analyzed (E, $n = 4$; $^*p < 0.05$ versus Ctrl group, one-way ANOVA, Bonferroni test). Scale bar, 100 μm.

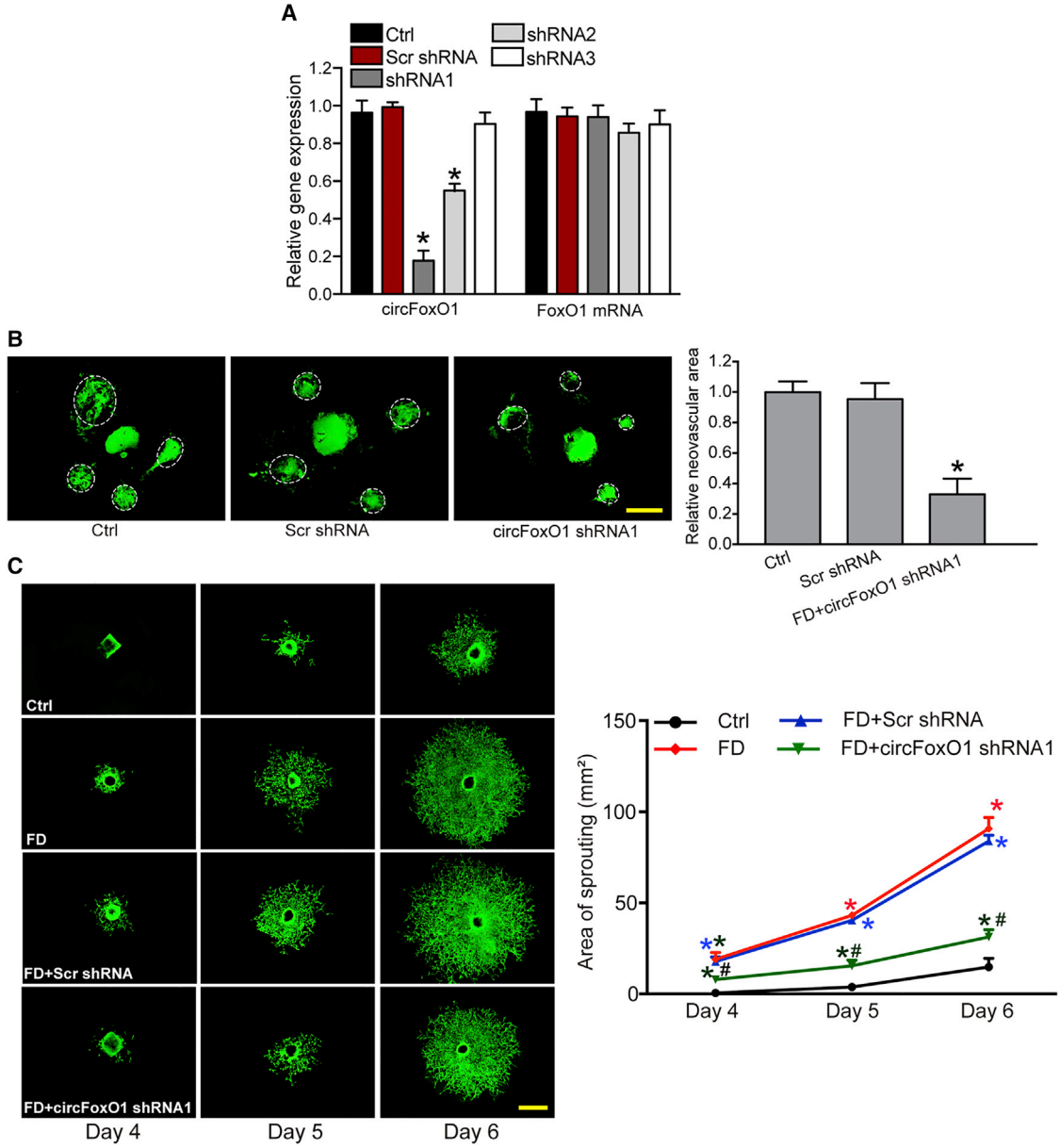

Figure 3. circFoxO1 regulates choroidal vascular dysfunction *in vivo* and *ex vivo*

(A) C57BL/6 mice (males, 8 weeks old) received an intravitreal injection of Scr shRNA, circFoxO1 shRNA1–3, or were left untreated (Ctrl) for 2 weeks. qRT-PCR assays were conducted to detect the levels of circFoxO1 and FoxO1 mRNA in choroid (n = 6; *p < 0.05 versus Ctrl group, Kruskal-Wallis test, Bonferroni test). (B) C57BL/6 mice received an intravitreal injection of Scr shRNA, circFoxO1 shRNA1, or were left untreated (Ctrl). Two weeks after laser injury, IB4 labeling was conducted to label the neovascular area in flat-mounted choroidal tissues. White circles denote the neovascular area (n = 6; *p < 0.05 versus Ctrl group, Kruskal-Wallis test, Bonferroni test). Scale bar, 100 μm. (C) Choroidal sprouting assays were conducted to determine the angiogenic potency of choroidal explants. CD31 staining was conducted to label choroidal sprouting. Representative images of choroidal sprouting and quantification results are shown (n = 6; *p < 0.05 versus Ctrl group; #p < 0.05 FD+Scr shRNA group versus FD+circFoxO1 shRNA1 group; Kruskal-Wallis test, Bonferroni test). Scale bar, 500 μm.

qRT-PCR assays showed that miR-145 expression was significantly reduced in myopic choroid compared with normal choroid (Figure 5E). Hypoxic stress or oxidative stress led to decreased miR-145 expression in RF/6A cells (Figure 5F). In addition, circFoxO1 overexpression led to decreased miR-145 expression in RF/6A cells (Figure 5G).

Next, we used TargetScan to predict the potential target genes of miR-145. Two candidate genes, VEGFA and ANGPT2, aroused our interest due to their roles in angiogenesis and retinopathy. miR-145 mimic transfection significantly downregulated VEGFA and ANGPT2 (Figure 5H). The 3′ untranslated region (UTR) of the VEGFA and

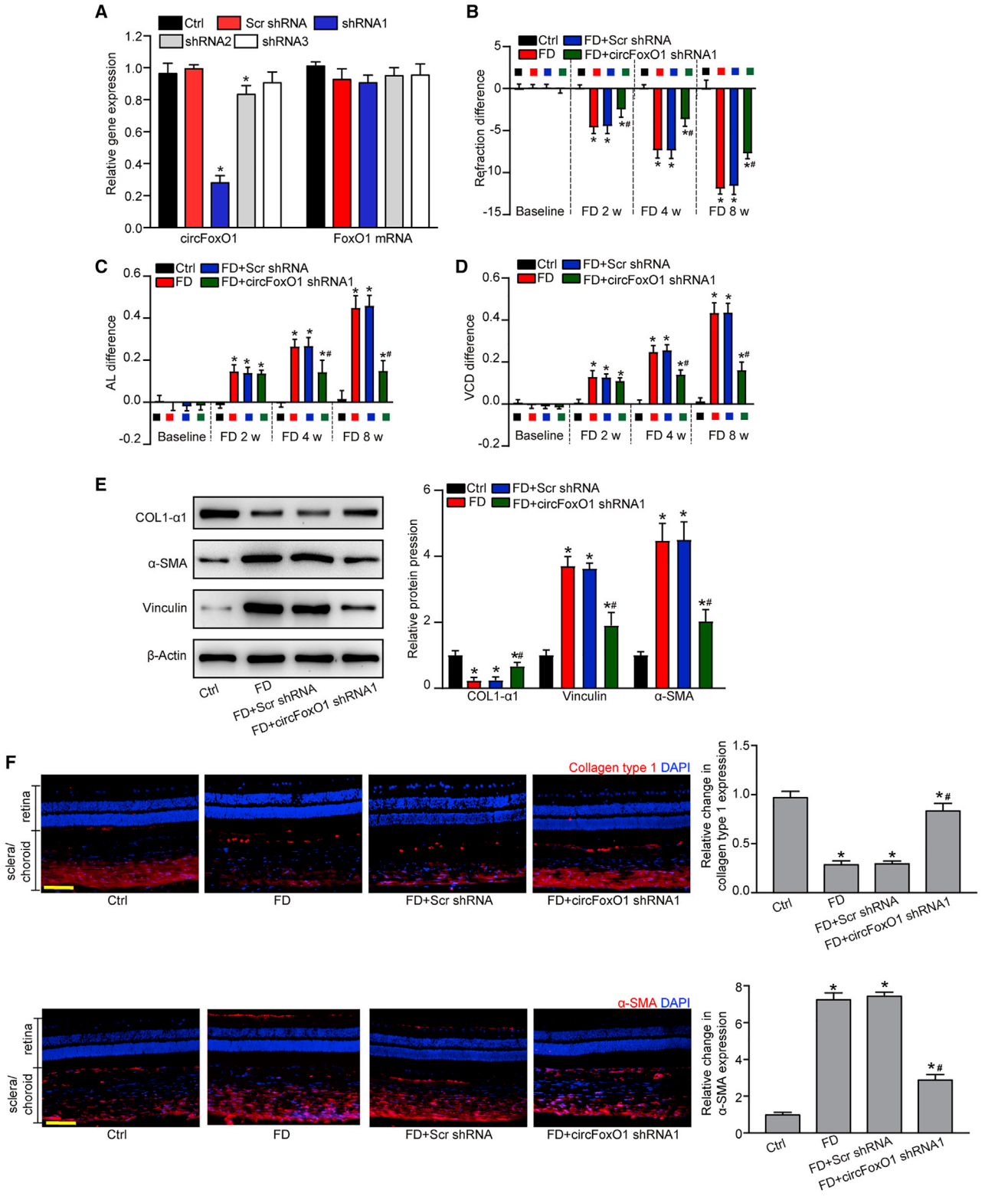

(legend on next page)

ANGPT2 genes was cloned into the luciferase vector and co-transfected with miR-145 mimic into HEK293T cells. A significant reduction in luciferase activity was detected in the presence of miR-145 mimic, whereas mutation of the miR-145 target site completely abolished this repression (Figure 5I).

The circFoxO1/miR-145/VEGFA or ANGPT2 axis regulates choroidal EC function *in vitro*

We subsequently investigated the role of miR-145 in choroidal ECs. MTT assays showed that miR-145 mimic transfection significantly decreased the viability of RF/6A cells compared with scramble miRNA transfection (Figure 6A). EdU assays showed that miR-145 mimic transfection significantly led to decreased cell proliferation (Figure 6B). Transwell and Matrigel tube formation assays showed that miR-145 mimic transfection significantly reduced the migration and tube formation ability of RF/6A cells (Figures 6C and 6D). miR-145 mimic could mimic the effects of circFoxO1 silencing on RF/6A cell function. Moreover, circFoxO1 overexpression could abrogate miR-145-mediated anti-angiogenic effects in RF/6A cells (Figures 6A–6D). We also showed that exogenous VEGFA or ANGPT2 overexpression could partially reverse the anti-angiogenic effects of circFoxO1 silencing in RF/6A cells (Figure S4). Collectively, these results suggest that the circFoxO1/miR-145/VEGFA or ANGPT2 axis is involved in the regulation of choroidal EC function *in vitro*.

We also determined the role of miR-145 in primarily isolated choroidal ECs. miR-145 mimic transfection could decrease the viability, proliferation, migration, and tube formation ability of choroidal ECs (Figure S5). miR-145 mimic could also mimic the effects of circFoxO1 silencing on choroidal EC function. circFoxO1 overexpression could abrogate miR-145-mediated anti-angiogenic effects on choroidal ECs (Figure S5).

The circFoxO1/miR-145/VEGFA or ANGPT2 axis regulates choroidal vascular dysfunction *in vivo*

We further investigated the role of the circFoxO1/miR-145/VEGFA or ANGPT2 axis in choroidal vascular dysfunction *in vivo*. circFoxO1 silencing led to decreased expression of VEGFA and ANGPT2 in choroid (Figure 7A). Injection of miR-145 agomir led to decreased expression of VEGFA and ANGPT2 in choroid from the laser-induced CNV model, which was consistent with the effect of circFoxO1 silencing on VEGFA and ANGPT2 expression (Figure 7B). Moreover, injection of miR-145 agomir significantly decreased the neovascular area in the choroidal flat mounts compared with the Scr shRNA-injected group (Figure 7C). In contrast, injection of miR-145 antagomir led to increased expression of VEGFA and ANGPT2 (Figure 7D) and increased neovascular area in the choroidal flat mounts compared with the Scr shRNA-injected group (Figure 7E).

DISCUSSION

Choroidal vascular dysfunction plays a critical role in the pathogenesis of myopia.[24,25] Understanding the cellular and functional changes in choriocapillary is essential for the prevention and management of myopia. In this study, we report a novel mechanism of choroid vascular dysfunction, which is regulated by a circRNA-mediated network. The level of circFoxO1 is significantly upregulated in myopic eyes. circFoxO1 silencing alleviates choroid vascular dysfunction, which can ultimately retard the progression of myopia.

The choroid is a highly vascularized layer, which is uniquely situated between the retina and the sclera.[26] The choroid can relay retina-derived signals to the sclera and affect scleral ECM remodeling and ocular size.[24] Accumulating clinical evidence has shown that myopia decreases the thickness of choroid.[27,28] In the present study, we identified a novel mechanism governing choroid vascular dysfunction. circFoxO1 overexpression may induce abnormal activation of ECs and accelerate choroid vascular dysfunction. Choroid vascular dysfunction may lead to decreased perfusion, inadequate oxygen supply, and tissue hypoxia. Hypoxia is shown as a critical inducer of ECM remodeling, which can result in decreased collagen production and ocular axial elongation.[9,21] In contrast, circFoxO1 silencing could alleviate choroid vascular dysfunction, improve choroidal vascular perfusion, and alleviate tissue hypoxia. Moreover, circFoxO1 silencing could reverse hypoxia-induced reduction of collagen and axial elongation. Thus, it is not surprising that circFoxO1 silencing can retard the progression of myopia.

Choroidal vascular defects contribute to the development of myopic pathologies; however, the molecular mechanisms underlying choroidal vascular dysfunction remain to be fully elucidated. Oxidative stress, hypoxic stress, inflammation, and mitochondrial dysfunction contribute to the development of choroidal pathologies.[11,29] Both oxidative stress and hypoxic stress can obviously lead to increased levels of circFoxO1 in myopic choroid tissue and choroidal ECs. Myopic pathologies are tightly associated with increased circFoxO1 levels. circFoxO1 silencing can alleviate choroidal vascular dysfunction and retard the progression of myopic pathology. ECs are the major cell types of choroidal vessels.[30] In pathological myopia, abnormal activation of ECs may lead to CNV.[31] circFoxO1 silencing can reduce the proliferation, mobility, and tube formation of choroidal ECs *in vitro*. We thus speculate that circFoxO1 deregulation is responsible for choroidal vascular dysfunction in myopia.

Figure 4. circFoxO1 silencing retards the progression of myopia *in vivo*

(A) The eyes of guinea pigs received an intravitreal injection of Scr shRNA, circFoxO1 shRNA1–3, or were left untreated (Ctrl) for 2 months. qRT-PCR assays were conducted to detect the levels of circFoxO1 (n = 6; *p < 0.05 versus Ctrl group, Kruskal-Wallis test, Bonferroni test). (B–D) Refraction difference (B), AL (C), and VCD (D) in guinea pigs after FD treatment was measured to determine the role of circFoxO1 in myopia. (E and F) The expression of a fibroblast marker (COL1α1) and myofibroblast markers (α-SMA and vinculin) in the sclera after circFoxO1 silencing were detected by western blot or immunofluorescence staining (n = 6; *p < 0.05 versus Ctrl group; #p < 0.05 FD+Scr shRNA group versus FD+circFoxO1 shRNA1 group; Kruskal-Wallis test, Bonferroni test). Scale bars, 100 μm.

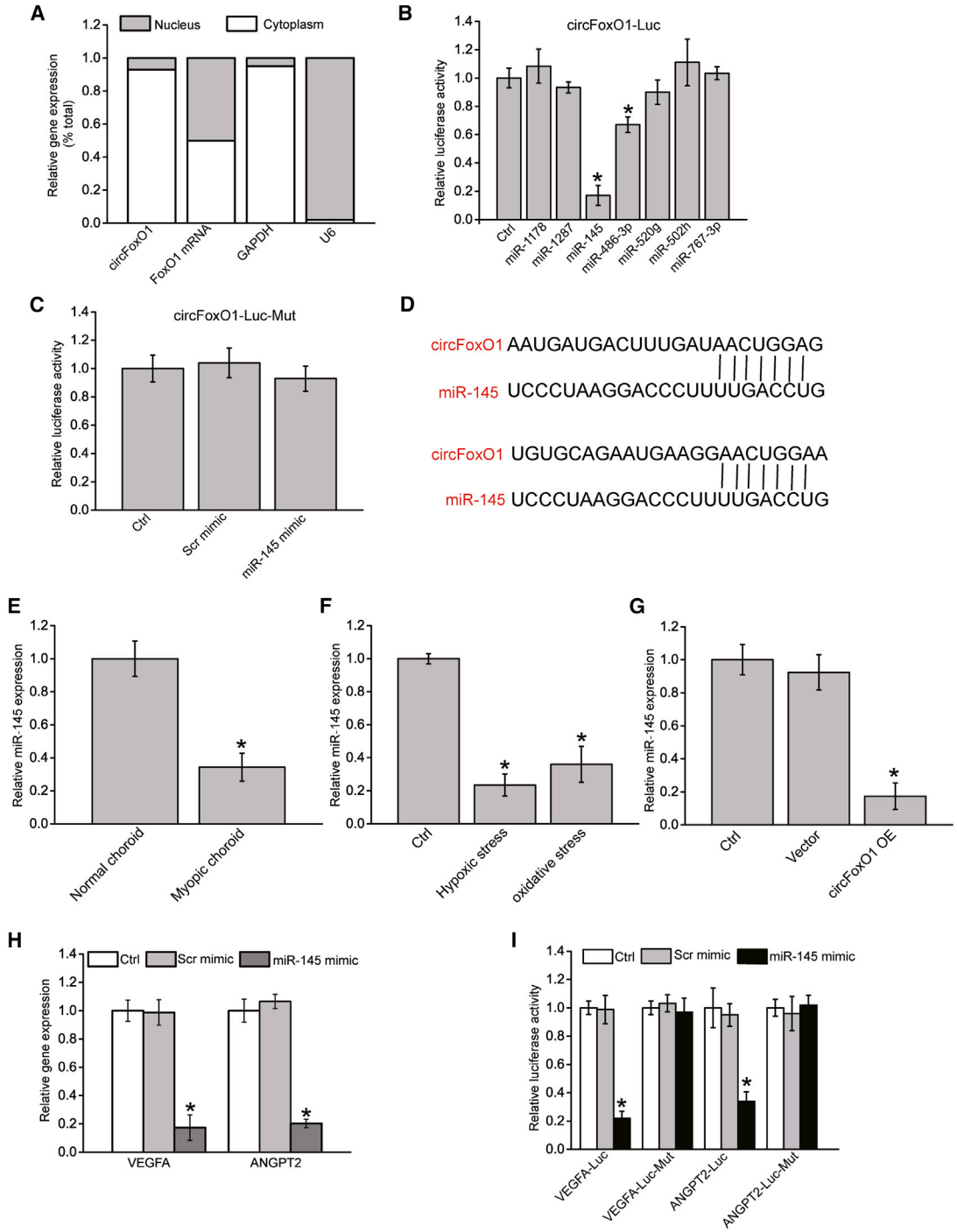

Figure 5. circFoxO1 acts as a miRNA sponge in choroidal ECs

(A) The expression of nucleus Ctrl transcript (U6), cytoplasmic Ctrl transcript (GAPDH), FoxO1 mRNA, and circFoxO1 was detected by qRT-PCRs in the nucleus and cytoplasmic fractions of RF/6A cells (n = 4). (B) The entire sequence of circFoxO1 was cloned into the pRL-TK luciferase reporter to construct the LUC-circFoxO1 vector. RF/6A cells were co-transfected LUC-circFoxO1 with different miRNA mimics. Luciferase activity was detected using a dual-luciferase assay 48 h after transfection (n = 4; *p < 0.05 versus Ctrl group, one-way ANOVA, Bonferroni test). (C) RF/6A cells were co-transfected LUC-circFoxO1-Mut (without miR-145 binding site) with miR-145 mimic, Scr mimics, or were left untreated (Ctrl). Luciferase activity was detected using a dual- luciferase assay at 48 h post-transfection (n = 4; *p < 0.05 versus Ctrl group, one-way ANOVA, Bonferroni test). (D) The putative binding sites of miR-145 on circFoxO1 transcript are shown. (E) qRT-PCR assays were conducted to detect the expression level of miR-145 in the choroidal tissues of C57BL/6 mice after 8-week FD induction (n = 6; *p < 0.05 versus normal choroid, Mann-Whitney U test, Bonferroni test). (F) RF/6A cells

(legend continued on next page)

circRNAs can regulate gene expression by affecting transcription, mRNA turnover, and translation by sponging RNA-binding proteins or miRNAs.[32] qRT-PCR assays show that circFoxO1 is mainly expressed in the cytoplasm of choroidal ECs, implicating that circFoxO1 regulates gene expression at the post-transcriptional level. circFoxO1 serves as a platform for Ago2 and miRNAs and acts as a sponge of miR-145. VEGFA and ANGPT2 are the potential target genes of miR-145. VEGFA is a critical EC-specific mitogen and an angiogenic inducer.[33] Increased VEGFA level has a mitogenic and anti-apoptotic effect on ECs. VEGF can increase vascular permeability and accelerate cell migration, and it contributes to normal and pathological angiogenesis.[34] ANGPT2 is an important proangiogenic cytokine and its upregulation contributes to angiogenesis and vascular inflammation.[35] Based on the above-mentioned evidence, we conclude that circFoxO1 acts as the sponge of miR-145, thereby inducing increased level of VEGFA and ANGPT2. circFoxO1 upregulation becomes a sink for miR-145 and eliminates the inhibitory function of miR-145 on VEGFA and ANGPT2. Collectively, the circFoxO1-miR-145-VEGFA/ANGPT2 axis is involved in choroidal vascular dysfunction.

In summary, this study provides important evidence that circFoxO1 serves as a novel regulator of choroidal vascular function by sponging miR-145. Targeting the circFoxO1-miR-145-VEGFA/ANGPT2 axis is a promising strategy for the prevention and management of myopic pathology.

MATERIALS AND METHODS

Animals

All animal treatments were conducted according to the Association for Research in Vision and Ophthalmology (ARVO) Statement for the Use of Animals in Ophthalmic and Vision Research. The animal research was approved by the Animal Care and Use Committee of the author's institute. They were reared in a temperature-controlled room with 12-h light/12-h dark cycles (on at 8:30 a.m., off at 8:30 p.m.) and allowed for free access to water and food with additional fresh vegetables every day as diet enrichment.

Induction of FD myopia

Three-week-old pigmented guinea pigs or 3-week-old male C57BL/6 mice were monocularly FD using the translucent eye shields. The contralateral eyes were taken as the controls. The shields were cleaned and checked every day. After FD treatment, 1% cyclopentolate (Cyclogyl; Alcon) was topically applied to each eye. The refractive errors were measured using a streak retinoscopy (66 Vision Tech, Jiangsu Province, China). VCD and AL were measured using an A-scan ultrasonography device.

Establishment of CNV model

For the induction of CNV, C57BL/6J mice (8 weeks old, males) were anesthetized through intraperitoneal injection of ketamine (80 mg/kg) and xylazine (4 mg/kg). After dilating pupils with tropicamide, four spots of laser photocoagulation in the posterior pole of retinas were created through the dilated pupil with a power of 120 mW, 100-μm-diameter spot size, and duration of 50 ms. The laser burns were produced in the 3, 6, 9, and 12 o'clock position around the optic disc and located approximately 3 disc-diameters away from the optic nerve head. The presence of bubble confirmed the disruption of Bruch's membrane.

Immunofluorescent staining

Frozen sections of the posterior eyecup were allowed to thaw and dry at room temperature for 30 min, and then fixed in 4% paraformaldehyde at 4°C for 20 min. The sections were blocked with 5% BSA for 30 min at room temperature, followed by incubating with the primary antibody at 4°C overnight and the secondary antibody for 3 h at room temperature. The cell nuclei were stained with 4′,6-diamidino-2-phenylindole (DAPI, 0.5 μg/mL) for 10 min.

Choroid sprouting assay

C57BL/6J mice were anesthetized by the intraperitoneal injection of ketamine (80 mg/kg) and xylazine (4 mg/kg) and euthanized by cervical dislocation. The eyes were carefully enucleated and kept in ice-cold medium before dissection. The retinal pigment epithelium (RPE)-choroid-sclera complex (choroid explants) was separated from the retina, and then the peripheral area of the optic nerve was cut into approximately 1.0 × 1.0-mm pieces. These explants were embedded in Matrigel (354230, BD Biosciences), seeded in 24-well tissue culture plates, and incubated at 37°C in 5% CO_2. About 800 μL of EGM-2 medium was added to each well, and the medium was changed every other day.

Quantitative reverse transcriptase PCR (qRT-PCR)

Total RNAs in tissues and cells were extracted using the TRIzol reagent (Invitrogen). RNA concentration was measured using the NanoDrop ND-1000 instrument (NanoDrop Technologies). Then, about 500 ng of RNAs was subjected for the synthesis of complementary DNAs (cDNAs) using a reverse transcriptase kit (Takara, China). qRT-PCRs were performed in 96-well plates using SYBR Premix Ex Taq II (Takara, Dalian, China). Each 20-μL reaction contained 10 μL of SYBR Green PCR master mix, 0.5 μL of each primer, 8 μL of double-distilled H_2O (ddH_2O), and 1 μL of cDNA. PCR conditions were

were incubated with normal culture medium, H_2O_2 (200 μM, oxidative stress), or $CoCl_2$ (100 μM, hypoxic stress) for 24 h. qRT-PCR assays were conducted to detect miR-145 expression (n = 4; *p < 0.05 versus Ctrl group, one-way ANOVA, Bonferroni test). (G) RF/6A cells were transfected with pcDNA3.1 (vector), pcDNA3.1-circFoxO1, or were left untreated (Ctrl) for 24 h. qRT-PCR assays were conducted to detect miR-145 expression levels (n = 4; *p < 0.05 versus Ctrl group, one-way ANOVA, Bonferroni test). (H) RF/6A cells were transfected with Scr mimic, miR-145 mimic, or were left untreated (Ctrl) for 24 h. qRT-PCR assays were conducted to detect VEGFA and ANGPT2 expression (n = 4; *p < 0.05 versus Ctrl group, one-way ANOVA, Bonferroni test). (I) RF/6A cells were co-transfected VEGFA-Luc, VEGFA-Luc mutant (Mut), ANGPT2-Luc, or ANGPT2-Luc Mut with Scr mimic, miR-145 mimic, or were left untreated (Ctrl) for 24 h. Luciferase activity was detected at 24 h post-transfection (n = 4; *p < 0.05 versus Ctrl group, one-way ANOVA, Bonferroni test).

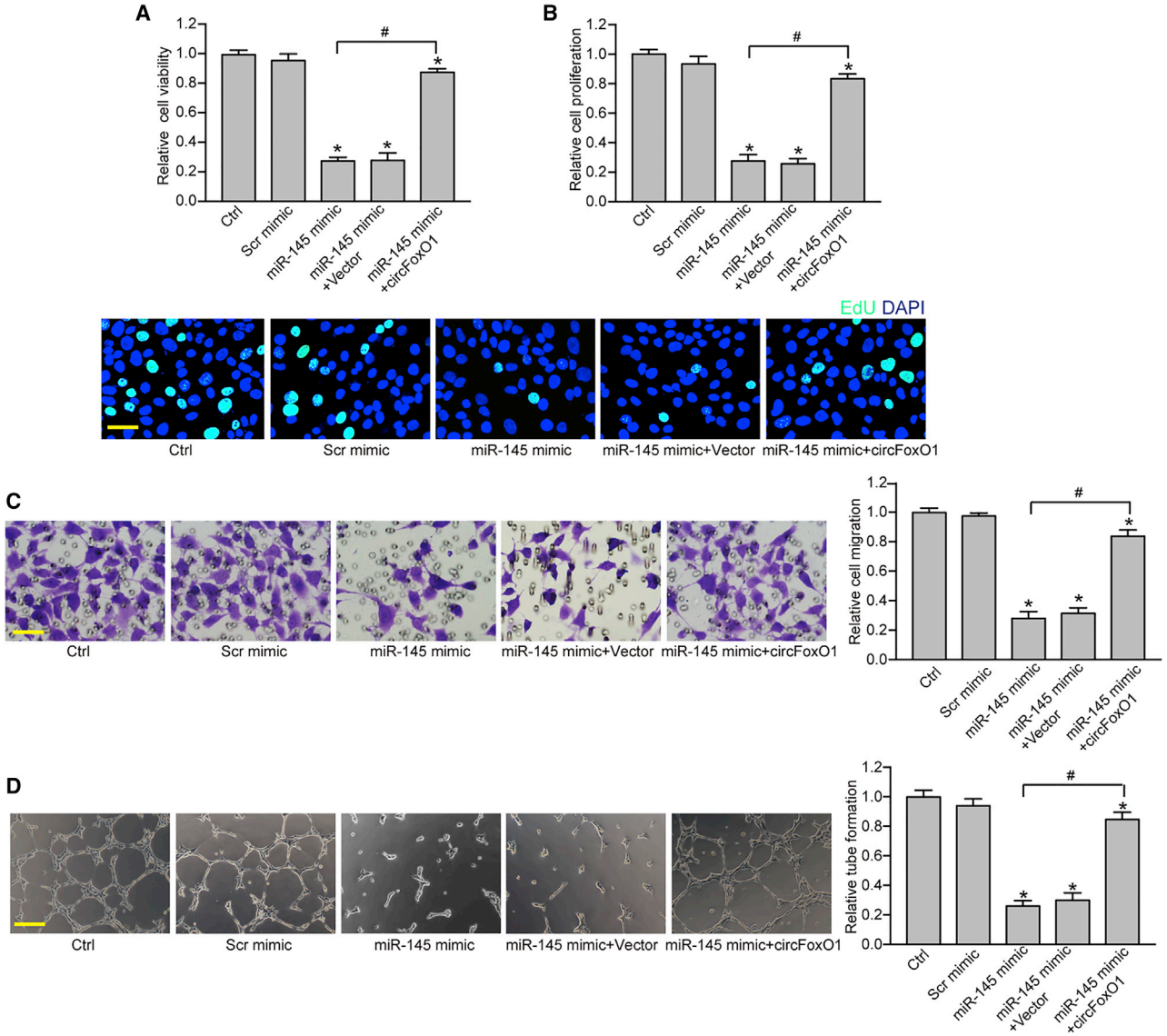

Figure 6. The circFoxO1/miR-145/VEGFA or ANGPT2 axis regulates choroidal EC function *in vitro*

(A) RF/6A cells were treated as shown. Cell viability was detected by an MTT assay (n = 4; *p < 0.05 versus Ctrl group, one-way ANOVA, Bonferroni test). (B) Cell proliferation was detected using EdU detection kits to analyze the incorporation of EdU during DNA synthesis (n = 4; *p < 0.05 versus Ctrl group, one-way ANOVA, Bonferroni test). A representative image along with the quantification result is shown. Scale bar, 20 μm. (C) Transwell assay and quantification analysis was conducted to determine the migration of RF/6A cells (n = 4; *p < 0.05 versus Ctrl group, one-way ANOVA, Bonferroni test). Representative images along with the quantification results are shown. Scale bar, 20 μm. (D) RF/6A cells were seeded on the Matrigel matrix. The tube-like structures were observed at 6 h after cell seeding. The average length of tube formation for each field was statistically analyzed (n = 4; *p < 0.05 versus Ctrl group, one-way ANOVA, Bonferroni test). Scale bar, 100 μm. *p < 0.05 versus Ctrl group; #p < 0.05 indicates significant difference between the marked group.

conducted as shown below: 95°C for 1 min, followed by 40 cycles at 95°C for 20 s, and 62°C for 30 s. The $2^{-\Delta\Delta Ct}$ method was used to calculate the relative expression of the target gene.

Western blot

Total proteins were extracted from the choroid and sclera samples using radioimmunoprecipitation assay (RIPA) lysis buffer (Beyotime Biotechnology) supplemented with protease inhibitor cocktail (4693159001; Roche). The concentration was measured using a bicinchoninic acid (BCA) protein assay (Beyotime Biotechnology). About 50 μg of proteins was separated on 10% SDS-PAGE for 1–2 h, and then transferred to polyvinylidene fluoride (PVDF) membranes (EMD Millipore). After blocking with non-fat milk, the PVDF membrane was incubated with the primary antibody against collagen type

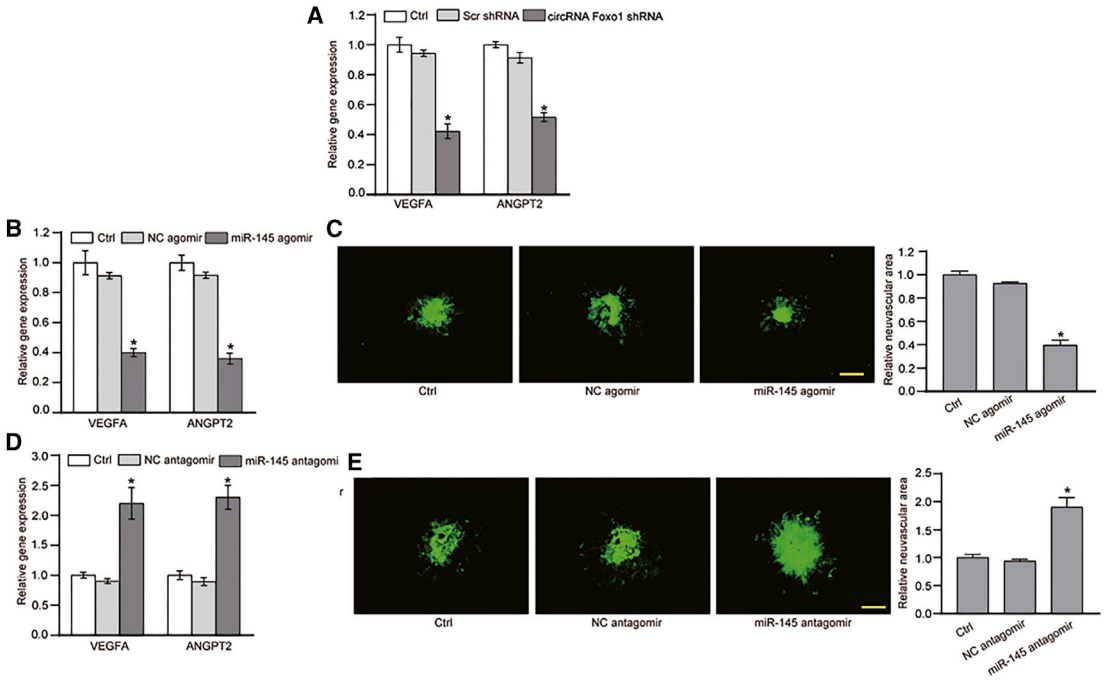

Figure 7. The circFoxO1/miR-145/VEGFA or ANGPT2 axis regulates choroidal vascular dysfunction *in vivo*

(A) C57BL/6 mice (males, 8 weeks old) received an intravitreal injection of Scr shRNA, circFoxO1 shRNA, or were left untreated (Ctrl) for 2 weeks. qRT-PCR assays were conducted to detect the levels of VEGFA and ANGPT2 in choroid. (B and C) C57BL/6 mice received an intravitreal injection of negative Ctrl (NC) agomir, miR-145 agomir, or were left untreated (Ctrl). Two weeks after laser injury, qRT-PCR assays were conducted to detect the levels of VEGFA and ANGPT2 in choroid. IB4 labeling was conducted to detect neovascular area in flat-mounted choroidal tissues. (D and E) C57BL/6 mice received an intravitreal injection of NC antagomir, miR-145 antagomir, or were left untreated (Ctrl). Two weeks after laser injuryqRT-PCR assays were conducted to detect the levels of VEGFA and ANGPT2 in choroid. IB4 labeling was conducted to detect neovascular area in flat-mounted choroidal tissues. n = 6; *p < 0.05 versus Ctrl group, Kruskal-Wallis test, Bonferroni test. Scale bars, 100 μm.

I (1:1,000, Abcam), α-SMA (1:2,000, Cell Signaling Technology), vinculin (1:1,000, Abcam), or β-actin (1:2,000, Abcam) overnight at 4°C. The membranes were then incubated with the secondary antibody for 2 h at room temperature. The protein bands were visualized by an enhanced chemiluminescence detection system. Quantification of protein bands were conducted using ImageJ software (National Institutes of Health).

Cell culture and transfection

RF/6A cells or choroidal ECs were cultured in Dulbecco's modified Eagle's medium (DMEM; Thermo Fisher Scientific) supplemented with 10% fetal bovine serum (FBS; Thermo Fisher Scientific) and 1% penicillin-streptomycin solution (Gibco) in a humidified incubator at 37°C in 5% CO_2. siRNAs directed against circFoxO1 and Scr siRNAs were synthesized by GenePharma (Shanghai, China). All transfections were performed using Lipofectamine 6000 (Beyotime Biotechnology, China) according to the manufacturer's instructions.

Isolation and culture of choroidal ECs

Choroidal ECs were isolated from one litter (six or seven pups) of 4-week-old C57BL/6J mice. Briefly, the eyes were enucleated, and the connective tissues were removed from the sclera. In cold DMEM, the anterior eye was removed, followed by the lens, vitreous, retina, and optic nerve, leaving RPE-choroid-sclera tissues. These tissues were minced into small pieces and digested using collagenase type I (1 mg/mL in serum free DMEM, Worthington Biochemical) for 30 min at 37°C. After digestion, DMEM with 10% FBS was added and cells were pelleted. Then, the cellular digests were filtered, centrifuged to pellet cells, and washed with DMEM containing 10% FBS. Finally, these cells were incubated with anti-platelet EC adhesion molecule 1 antibody-coated magnetic beads. The magnetic beads were washed, and the bound cells were choroidal ECs.

Cell viability assay

MTT assays were used to detect cell viability. Briefly, RF/6A cells (2×10^4) or choroidal ECs (2×10^4) were cultured in a 96-well plate and incubated for the indicated times. Then, 10 μL of MTT solution (5 mg/mL, Sigma-Aldrich) was added to each well and incubated at 37°C for 4 h. The formazan crystals were dissolved in 100 μL of DMSO. The absorbance was measured in the microreader at a wavelength of 570 nm (Thermo Scientific).

Cell proliferation assay

The EdU assay kit (Ribobio, Guangzhou, China) was used to determine cell proliferation. After the required treatment, RF/6A cells or choroidal ECs were incubated with 50 μM EdU reagent at 37°C for 2 h, fixed with 4% paraformaldehyde (Biosharp, China) for 30 min,

and permeabilized with 0.3% Triton X-100 for an additional 20 min. The staining results were observed using an inverted fluorescence microscope (Olympus, Tokyo, Japan).

Cell migration assay

A transwell assay was used to determine the ability of cell migration. Briefly, the transwell chamber with 8.0-μm pores (Corning Life Sciences, NY, USA) was placed on a 24-well plate. RF/6A cells or choroidal ECs were plated at a density of 1×10^4 cells per chamber into the upper chamber. DMEM supplemented with 10% FBS was added to the lower chamber as a chemoattractant. After 12 h, these non-migrated cells were removed from the upper surface and the filters were stained with crystal violet.

Tube formation assay

BD Matrigel matrix gel was seeded in 24-well culture plates and placed in an incubator at 37°C for 30 min. RF/6A cells or choroidal ECs were added to each well when the gel was solidified. They were then cultured at 37°C for 6 h. Tube formation was quantified by ImageJ software.

Cytoplasm/nucleus fraction isolation

Cytoplasm/nucleus fraction percentage was detected using a nuclear/cytosol fractionation kit (Cell Biolabs). Briefly, the extracted RNAs from the cytoplasm or nucleus were detected using qRT-PCRs. Relative expression levels of circFoxO1, FoxO1 mRNA, nuclear control transcript (U6), and cytoplasmic control transcript (GAPDH) were determined.

Luciferase assay

Luciferase assays were conducted using a luciferase assay kit (Promega, Madison, WI, USA) according to the manufacturer's protocols. Briefly, HEK293T cells were seeded in 24-well plates at 80% confluence. The wild-type or the mutant 3′ untranslated region of VEGFA, ANGPT2, or the circFoxO1 sequence was constructed and cloned into the pRL-TK plasmid (Promega) vector. Then, the cells were co-transfected with miRNA mimics using Lipofectamine 6000 (Beyotime Technology, China). After 48 h, the firefly and Renilla luciferase activities were detected using a luciferase assay kit.

Statistical analysis

All data are presented as mean ± standard error of the mean (SEM). Statistical analysis was performed using GraphPad Prism software. For normally distributed data with equal variance, the significance was determined by a Student's t test (two-group comparisons) or one-way ANOVA (multi-group comparisons) followed by Bonferroni's multiple comparison post hoc test. For non-normally distributed data or data with unequal variances, the significance was determined by a Mann-Whitney U test (two-group comparisons) or Kruskal-Wallis test followed by Bonferroni's post hoc test (multi-group comparisons). $p < 0.05$ was considered statistically significant.

SUPPLEMENTAL INFORMATION

Supplemental information can be found online at https://doi.org/10.1016/j.ymthe.2021.02.025.

ACKNOWLEDGMENTS

This work was generously supported by grants from the National Natural Science Foundation of China (grant no. 81470594 to B.Y.) and the Shanghai Youth Talent Support Program (to B.Y.).

AUTHOR CONTRIBUTIONS

The concept was set up by B.Y. and Y.L. Design and approach of experiments were performed by D.L., C.L., Y.-N.S., C.-Y.Z., and S.-S.X. Experiments and setup of methods were done by C.L., S.-S.X., K.S., and S.-J.Z. Data analysis was done by C.L., Y.-N.S., and S.-S.X. B.Y. designed and drafted the manuscript. The manuscript was reviewed by all authors.

DECLARATION OF INTERESTS

The authors declare no competing interests.

REFERENCES

1. Morgan, I.G., Ohno-Matsui, K., and Saw, S.M. (2012). Myopia. Lancet *379*, 1739–1748.
2. Bressler, N.M. (2020). Reducing the progression of myopia. JAMA *324*, 558–559.
3. Morgan, I.G., French, A.N., Ashby, R.S., Guo, X., Ding, X., He, M., and Rose, K.A. (2018). The epidemics of myopia: aetiology and prevention. Prog. Retin. Eye Res. *62*, 134–149.
4. Li, Y., Zhang, Y., Li, P., Mi, G., Tu, J., Sun, L., Webster, T.J., and Shen, Y. (2017). Ion-paired pirenzepine-loaded micelles as an ophthalmic delivery system for the treatment of myopia. Nanomedicine (Lond.) *13*, 2079–2089.
5. Barsam, A., and Allan, B.D. (2014). Excimer laser refractive surgery versus phakic intraocular lenses for the correction of moderate to high myopia. Cochrane Database Syst. Rev. (6), CD007679.
6. Hiraoka, T., Kakita, T., Okamoto, F., and Oshika, T. (2015). Influence of ocular wavefront aberrations on axial length elongation in myopic children treated with overnight orthokeratology. Ophthalmology *122*, 93–100.
7. Kiefer, A.K., Tung, J.Y., Do, C.B., Hinds, D.A., Mountain, J.L., Francke, U., and Eriksson, N. (2013). Genome-wide analysis points to roles for extracellular matrix remodeling, the visual cycle, and neuronal development in myopia. PLoS Genet. *9*, e1003299.
8. Bikbov, M.M., Gilmanshin, T.R., Kazakbaeva, G.M., Zainullin, R.M., Rakhimova, E.M., Rusakova, I.A., Bolshakova, N.I., Safiullina, K.R., Zaynetdinov, A.F., Zinatullin, A.A., et al. (2020). Prevalence of myopic maculopathy among adults in a Russian population. JAMA Netw. Open *3*, e200567.
9. Wu, H., Chen, W., Zhao, F., Zhou, Q., Reinach, P.S., Deng, L., Ma, L., Luo, S., Srinivasalu, N., Pan, M., et al. (2018). Scleral hypoxia is a target for myopia control. Proc. Natl. Acad. Sci. USA *115*, E7091–E7100.
10. Yu, D.Y., Yu, P.K., Cringle, S.J., Kang, M.H., and Su, E.N. (2014). Functional and morphological characteristics of the retinal and choroidal vasculature. Prog. Retin. Eye Res. *40*, 53–93.
11. Zhu, Y., Zhang, T., Xu, G., and Peng, L. (2016). Anti-vascular endothelial growth factor for choroidal neovascularisation in people with pathological myopia. Cochrane Database Syst. Rev. *12*, CD011160.
12. Labrousse-Arias, D., Martínez-Ruiz, A., and Calzada, M.J. (2017). Hypoxia and redox signaling on extracellular matrix remodeling: from mechanisms to pathological implications. Antioxid. Redox Signal. *27*, 802–822.
13. Kristensen, L.S., Andersen, M.S., Stagsted, L.V.W., Ebbesen, K.K., Hansen, T.B., and Kjems, J. (2019). The biogenesis, biology and characterization of circular RNAs. Nat. Rev. Genet. *20*, 675–691.
14. Chen, L.L. (2016). The biogenesis and emerging roles of circular RNAs. Nat. Rev. Mol. Cell Biol. *17*, 205–211.
15. Li, X., Yang, L., and Chen, L.L. (2018). The biogenesis, functions, and challenges of circular RNAs. Mol. Cell *71*, 428–442.

16. Dube, U., Del-Aguila, J.L., Li, Z., Budde, J.P., Jiang, S., Hsu, S., Ibanez, L., Fernandez, M.V., Farias, F., Norton, J., et al.; Dominantly Inherited Alzheimer Network (DIAN) (2019). An atlas of cortical circular RNA expression in Alzheimer disease brains demonstrates clinical and pathological associations. Nat. Neurosci. *22*, 1903–1912.

17. Aufiero, S., Reckman, Y.J., Pinto, Y.M., and Creemers, E.E. (2019). Circular RNAs open a new chapter in cardiovascular biology. Nat. Rev. Cardiol. *16*, 503–514.

18. Vo, J.N., Cieslik, M., Zhang, Y., Shukla, S., Xiao, L., Zhang, Y., Wu, Y.M., Dhanasekaran, S.M., Engelke, C.G., Cao, X., et al. (2019). The landscape of circular RNA in cancer. Cell *176*, 869–881.e13.

19. Nickla, D.L., and Wallman, J. (2010). The multifunctional choroid. Prog. Retin. Eye Res. *29*, 144–168.

20. Milani, P., Montesano, G., Rossetti, L., Bergamini, F., and Pece, A. (2018). Vessel density, retinal thickness, and choriocapillaris vascular flow in myopic eyes on OCT angiography. Graefes Arch. Clin. Exp. Ophthalmol. *256*, 1419–1427.

21. Zhao, F., Zhang, D., Zhou, Q., Zhao, F., He, M., Yang, Z., Su, Y., Zhai, Y., Yan, J., Zhang, G., et al. (2020). Scleral HIF-1α is a prominent regulatory candidate for genetic and environmental interactions in human myopia pathogenesis. EBioMedicine *57*, 102878.

22. Yuan, Y., Li, M., To, C.H., Lam, T.C., Wang, P., Yu, Y., Chen, Q., Hu, X., and Ke, B. (2018). The role of the RhoA/ROCK signaling pathway in mechanical strain-Induced scleral myofibroblast differentiation. Invest. Ophthalmol. Vis. Sci. *59*, 3619–3629.

23. Hansen, T.B., Jensen, T.I., Clausen, B.H., Bramsen, J.B., Finsen, B., Damgaard, C.K., and Kjems, J. (2013). Natural RNA circles function as efficient microRNA sponges. Nature *495*, 384–388.

24. Summers, J.A. (2013). The choroid as a sclera growth regulator. Exp. Eye Res. *114*, 120–127.

25. Zhang, Y., and Wildsoet, C.F. (2015). RPE and choroid mechanisms underlying ocular growth and myopia. Prog. Mol. Biol. Transl. Sci. *134*, 221–240.

26. Borrelli, E., Sarraf, D., Freund, K.B., and Sadda, S.R. (2018). OCT angiography and evaluation of the choroid and choroidal vascular disorders. Prog. Retin. Eye Res. *67*, 30–55.

27. Read, S.A., Alonso-Caneiro, D., Vincent, S.J., and Collins, M.J. (2015). Longitudinal changes in choroidal thickness and eye growth in childhood. Invest. Ophthalmol. Vis. Sci. *56*, 3103–3112.

28. Ho, M., Liu, D.T., Chan, V.C., and Lam, D.S. (2013). Choroidal thickness measurement in myopic eyes by enhanced depth optical coherence tomography. Ophthalmology *120*, 1909–1914.

29. Neelam, K., Cheung, C.M., Ohno-Matsui, K., Lai, T.Y., and Wong, T.Y. (2012). Choroidal neovascularization in pathological myopia. Prog. Retin. Eye Res. *31*, 495–525.

30. Lutty, G.A., and McLeod, D.S. (2018). Development of the hyaloid, choroidal and retinal vasculatures in the fetal human eye. Prog. Retin. Eye Res. *62*, 58–76.

31. Wang, H., Ramshekar, A., Kunz, E., Sacks, D.B., and Hartnett, M.E. (2020). IQGAP1 causes choroidal neovascularization by sustaining VEGFR2-mediated Rac1 activation. Angiogenesis *23*, 685–698.

32. Zlotorynski, E. (2019). The innate function of circular RNAs. Nat. Rev. Mol. Cell Biol. *20*, 387.

33. Ferrara, N. (2004). Vascular endothelial growth factor: basic science and clinical progress. Endocr. Rev. *25*, 581–611.

34. Sene, A., Chin-Yee, D., and Apte, R.S. (2015). Seeing through VEGF: innate and adaptive immunity in pathological angiogenesis in the eye. Trends Mol. Med. *21*, 43–51.

35. Akwii, R.G., Sajib, M.S., Zahra, F.T., and Mikelis, C.M. (2019). Role of angiopoietin-2 in vascular physiology and pathophysiology. Cells *8*, 471.

YMTHE, Volume *29*

Supplemental Information

Targeting choroidal vascular dysfunction via inhibition of circRNA-FoxO1 for prevention and management of myopic pathology

Dan Li, Chang Liu, Ya-Nan Sun, Chuan-Yan Zhu, Shan-Shan Xu, Kun Shan, Shu-Jie Zhang, Biao Yan, and Yi Lu

Supplementary Material

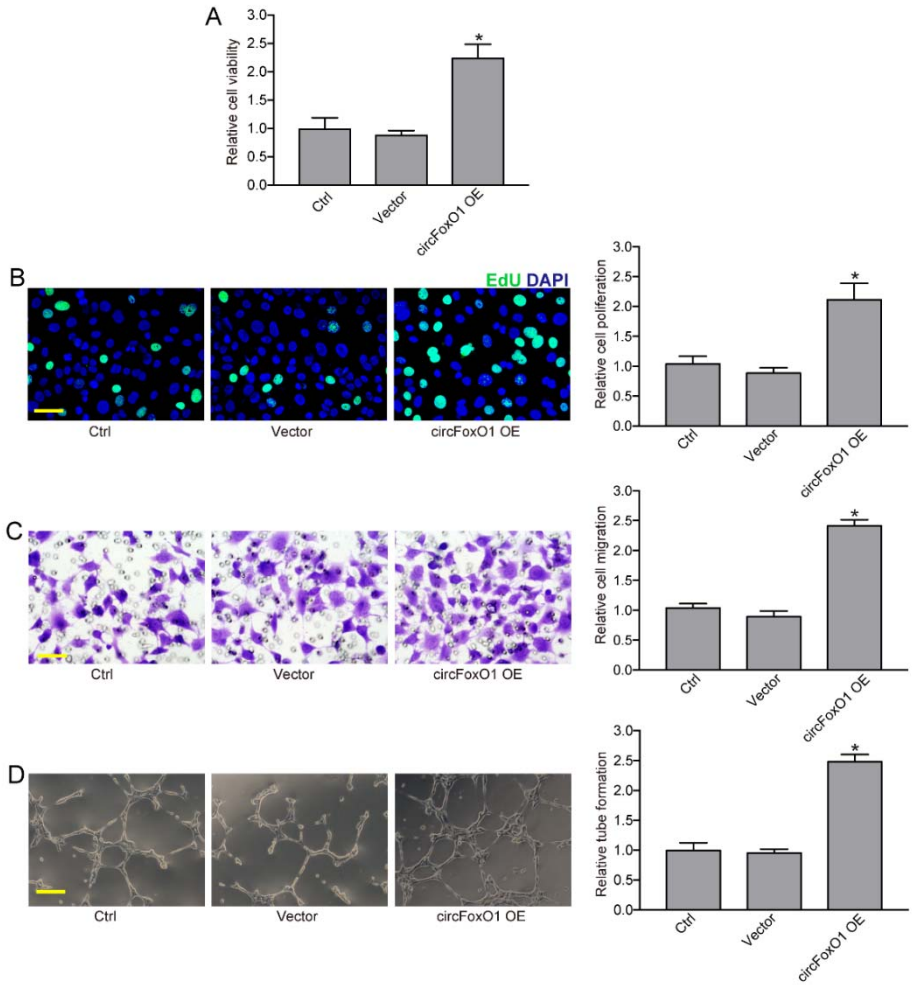

Figure S1. circFoxO1 overexpression is capable of driving angiogenic phenotypes in RF/6A cells. (A-D) RF/6A cells were transfected with pcDNA3.1 (Vector), pcDNA3.1-circFoxO1 (OE), or left untreated (Ctrl) for 48 h. MTT assays were conducted to detect cell viability (A, n=4, **P*<0.05 vs. Ctrl group, 1-way ANOVA, Bonferroni test). Cell proliferation was detected using the EdU detection kit (B, n=4, **P*<0.05 vs. Ctrl group, 1-way ANOVA, Bonferroni test, Scale bar: 20 μm). The migration ability of RF/6A cells was determined by Transwell assay. The cells that migrated through the Transwell were quantified (C, n=4, **P*<0.05 vs. Ctrl group, 1-way ANOVA, Bonferroni test, Scale bar: 20 μm). The tube-like structures were observed 6 h after cell seeding on the matrigel matrix and average length of tube formation for each field was statistically analyzed (D, n=4, **P*<0.05 vs. Ctrl group, 1-way ANOVA, Bonferroni test, Scale bar:100 μm).

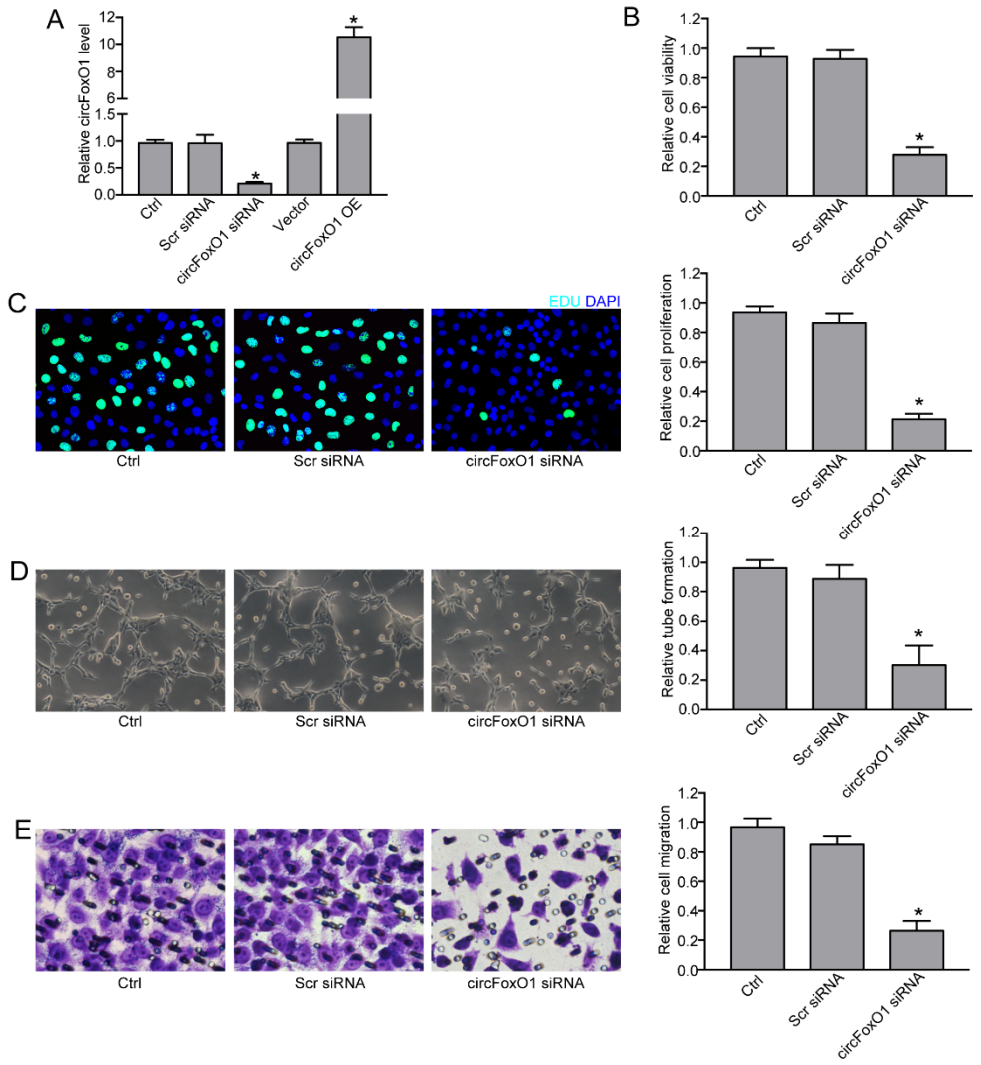

Figure S2. circFoxO1 regulates choroidal endothelial cell function in vitro. (A) Choroidal ECs were transfected with scrambled (Scr) siRNA, circFoxO1 siRNA, pcDNA 3.1 vector, pcDNA 3.1-circFoxO1 (circFoxO1 OE), or left untreated (Ctrl) for 48 h. qRT-PCR assays were conducted to detect the level of circFoxO1 (n=4, **P*<0.05 vs. Ctrl group, 1-way ANOVA, Bonferroni test). (B-E) Choroidal ECs were transfected with scrambled (Scr) siRNA, circFoxO1 siRNA, or left untreated (Ctrl) for 48 h. Cell viability was detected using MTT assay (B, n=4, **P*<0.05 vs. Ctrl group, 1-way ANOVA, Bonferroni test). Cell proliferation was detected using EdU detection kit to analyze the incorporation of EdU during DNA synthesis. (C, n=4, **P*<0.05 vs. Ctrl group, 1-way ANOVA, Bonferroni test, Scale bar: 20 μm). The cells were seeded on the matrigel matrix. The tube-like structures were observed 6 h after cell seeding. The average length of tube formation for each field was statistically analyzed (D, n=4, **P*<0.05 vs. Ctrl group, 1-way ANOVA, Bonferroni test, Scale bar: 100 μm).The migration was determined using the transwell assay and the cells that migrated through the transwell were quantified. (E, **P*<0.05 vs. Ctrl group, 1-way ANOVA, Bonferroni test, Scale bar: 20 μm).

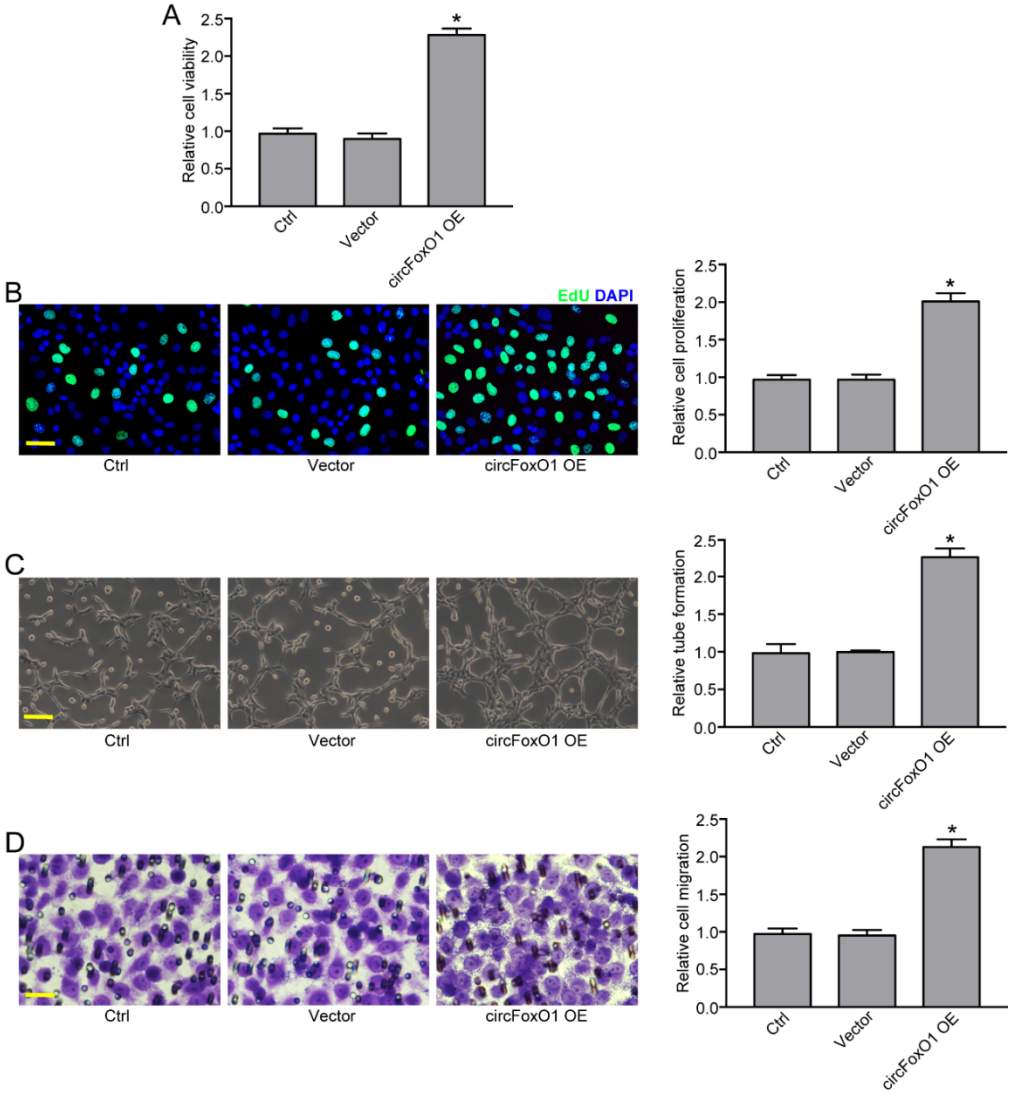

Figure S3. circFoxO1 overexpression is capable of driving angiogenic phenotypes in choroidal ECs. (A-D) Choroidal ECs (CECs) were transfected with pcDNA3.1 (Vector), pcDNA3.1-circFoxO1 (OE), or left untreated (Ctrl) for 48 h. MTT assays were conducted to detect cell viability (A, n=4, **P*<0.05 vs. Ctrl group, 1-way ANOVA, Bonferroni test). Cell proliferation was detected using the EdU detection kit (B, n=4, **P*<0.05 vs. Ctrl group, 1-way ANOVA, Bonferroni test, Scale bar: 20 μm). The tube-like structures were observed 6 h after cell seeding on the matrigel matrix and average length of tube formation for each field was statistically analyzed (C, n=4, **P*<0.05 vs. Ctrl group, 1-way ANOVA, Bonferroni test; Scale bar:100 μm). The migration ability was determined by Transwell assay. The cells that migrated through the Transwell were quantified. (D, n=4, **P*<0.05 vs. Ctrl group, 1-way ANOVA, Bonferroni test; Scale bar: 20 μm).

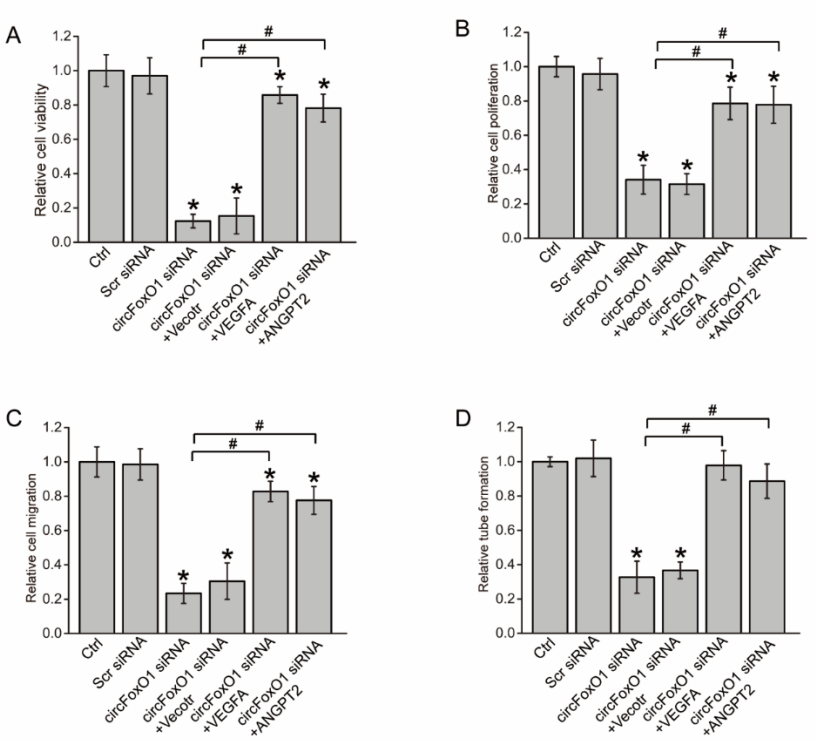

Figuew S4. circFoxO1-VEGFA or ANGPT2 crosstalk regulates endothelial cell function in vitro. (A) RF/6A cells were treated as shown. Cell viability was determined using MTT assay (n=4, 1-way ANOVA, Bonferroni test). (B) Cell proliferation was detected using EdU kits (n=4, 1-way ANOVA, Bonferroni test). The quantification result was shown. (C) Transwell assay and quantification analysis was conducted to detect the migration ability of RF/6A cells (n=4, 1-way ANOVA, Bonferroni test). (D) RF/6A cells were seeded on the matrigel matrix. The tube-like structures were observed 6 h after cell seeding. The average length of tube formation for each field was statistically analyzed (n=4, 1-way ANOVA, Bonferroni test). **P*<0.05 versus Ctrl group; $^{\#}$*P*<0.05 indicated significant difference between the marked group.

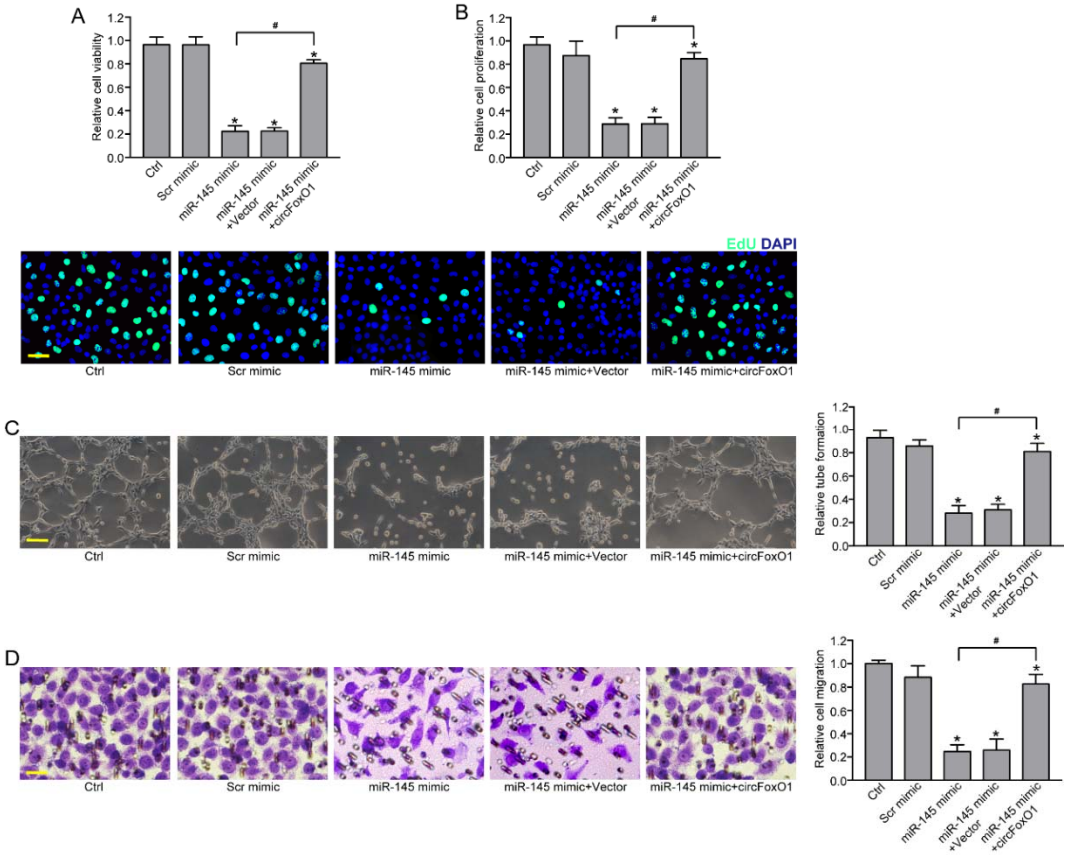

Figure S5. circFoxO1/miR-145/VEGFA or ANGPT2 axis regulates choroidal EC function. (A) The primarily isolated choroidal ECs were treated as shown. Cell viability was detected by MTT assay (n=4, 1-way ANOVA, Bonferroni test). (B) Cell proliferation was detected using EdU detection kits (n=4, 1-way ANOVA, Bonferroni test, Scale bar: 20 μm). A representative image along with the quantification result was shown. (C) Choroidal ECs were seeded on the matrigel matrix. The tube-like structures were observed at 6 h after cell seeding. The average length of tube formation for each field was statistically analyzed (n=4, 1-way ANOVA, Bonferroni test, Scale bar: 100 μm). (D) Transwell assay and quantification analysis was conducted to determine cell migration (n=4, **P*<0.05 vs. Ctrl group, 1-way ANOVA, Bonferroni test, Scale bar: 20 μm). The representative images along with the quantification results were shown. **P*<0.05 versus Ctrl group; $^{\#}$*P*<0.05 indicated significant difference between the marked group.